This is a repository copy of *Utilization of stochastically located customer owned battery energy storage systems for violation management on UK LV residential feeders with varying renewables penetrations*.

White Rose Research Online URL for this paper:
http://eprints.whiterose.ac.uk/134025/

Version: Accepted Version

Article:
Johnson, R.C., Mayfield, M. orcid.org/0000-0002-9174-1773 and Beck, S.B.M. orcid.org/0000-0003-2673-4179 (2018) Utilization of stochastically located customer owned battery energy storage systems for violation management on UK LV residential feeders with varying renewables penetrations. Journal of Energy Storage, 19. pp. 52-66. ISSN 2352-152X

https://doi.org/10.1016/j.est.2018.07.005

Article available under the terms of the CC-BY-NC-ND licence (https://creativecommons.org/licenses/by-nc-nd/4.0/).

Reuse
This article is distributed under the terms of the Creative Commons Attribution-NonCommercial-NoDerivs (CC BY-NC-ND) licence. This licence only allows you to download this work and share it with others as long as you credit the authors, but you can't change the article in any way or use it commercially. More information and the full terms of the licence here: https://creativecommons.org/licenses/

Takedown
If you consider content in White Rose Research Online to be in breach of UK law, please notify us by emailing eprints@whiterose.ac.uk including the URL of the record and the reason for the withdrawal request.

eprints@whiterose.ac.uk
https://eprints.whiterose.ac.uk/

Utilization of stochastically located customer owned battery energy storage systems for violation management on UK LV residential feeders with varying renewables penetrations

R.C. Johnson[a], M. Mayfield[a], S.B.M. Beck[b]

[a]Department of Civil and Structural Engineering, University of Sheffield, UK

[b]Department of Mechanical Engineering, University of Sheffield, UK

Corresponding author: R. C. Johnson

Email: RCJohnson2@sheffield.ac.uk

Address: 44 Lavender Way, Wincobank, Sheffield, S5 6DH

Conflicts of Interest: None

Abstract

As the installed capacity of residential rooftop PV systems increases in the UK, the likelihood that LV networks will experience periods of unacceptably high voltage or line utilization increases also. Whilst the use of battery energy storage systems (BESSs) for violation management has been explored in previous work, the robustness and cost effectiveness of utilizing existing customer owned BESSs for such purposes has not been extensively examined on UK LV networks. In this paper, we use mixed-integer quadratically constrained programming (MIQCP) formulations to determine optimal BESS takeover for violation control at various PV and ASHP ownership fractions, whilst implementing Monte-Carlo methods to explore the multiple possible technology ownership patterns that may occur at each penetration level. We compare the cost of feasible BESS takeover solutions to the cost of the reconductoring works that would be required to mitigate the same violations, where novel mixed integer linear programming (MILP) formulations are used to determine the optimum reconductoring strategies. We perform the analysis on two models of real urban feeders located in the north west of England, and find that whilst BESS control may sometimes compete economically with reconductoring, BESS takeover control cannot consistently and adequately mitigate violations at the majority of PV and ASHP ownership fractions when BESSs are available at fewer than 100% of PV array owners residences.

Keywords: Energy storage, LV networks, PV, ASHP, optimization

1 Introduction

With increasing concern for the security and environmental sustainability of the UK energy supply, the penetration of low carbon technologies on the grid has increased significantly, with the most recently available figures suggesting a total installed capacity of 12.7 GW solar photovoltaic (PV) [1] and approximately 100,000 individual domestic heat pump systems [2]. Though rooftop PV installation rate in the UK has fallen since a recent feed in tariff reduction [3], a 60% reduction in system costs over coming decades (resulting from technological advances in silicon solar cell development [4], multi-junction cell research [5], and productivity increases as a result of industry learning [6]) is predicted, and sources suggest that an 18% - 25% penetration increase by 2035 is possible [7]. Furthermore, it is predicted that up to 1 million homes may own air source heat pump (ASHP) systems by 2035 [7].

As the penetration of low carbon technologies on UK LV networks increases, the likelihood that voltage and line ampacity violations will be observed at times of high generation or high demand also increases [8]. Many approaches have been explored in literature, including reconductoring networks with lower impedance, higher ampacity cabling [9], injecting leading/lagging reactive power via PV or BESS inverters [10], [11], and charging or discharging real power using BESSs [9], [10], [12]. Much of the technology required to implement a BESS based strategy has become commonplace over recent years, with small scale residential BESSs such as the Tesla Powerwall [13], and bidirectional inverter systems [14], [15], now commercially available to the consumer. Methods for coupling PV and BESS systems to the wider grid are well documented and understood [16], and the range of operating modes accessible on commercially available inverter systems is increasing; most commercially available bidirectional inverters are now able to operate at non unity power factors, and development of inverters capable of interacting with grid signals to provide load shifting, frequency and voltage control, feed in limiting, and harmonics compensation services is progressing [17]–[19].

Previous work has considered how customer owned BESSs may be controlled to alleviate violations on typical European LV networks. Marra et al. considered a decentralized feed-in-limit (FIL) based placement and control approach that triggers BESSs based on the power threshold at which voltage issues begin to occur. The algorithm is applied over a simulation period of one year on a modelled Belgian LV feeder with 20% PV penetration, and adequate control is observed [20]. However, PV placement is not considered probabilistically, and the simulation is performed at only one penetration level. Wang et al [21] present schemes in which customer owned BESSs are time shared between DNOs (for voltage and utilization control) and residents (for increased self-consumption), and Ranaweera [22], suggests a similar scheme in which customer BESSs are taken over by the

DNO to provide voltage and utilization support on a network with 40% PV ownership and 7% BESS ownership. Again, both studies only consider a single technology penetration and placement.

Procopiou (2017) [12], considers an advanced decentralized residential BESS control scheme. BESSs may charge only during peak PV generation hours, charging is limited to ensure enough energy capacity remains for voltage control, and a FIL is determined for each BESS (which is approximated as the export limit at which voltage issues may arise). Furthermore, simulations are performed at each PV penetration level to account for the effect of changes in array location, size, and load demand on results. The algorithm is applied to a French LV network, and is shown to work effectively up to PV penetrations of 60%, at which point customers begin to experience overvoltage problems. However, this assumes that every PV owner also owns a Tesla Powerwall system that they are willing to offer to the FIL scheme. Lamberti et al. performed a similar study using an Italian feeder model which allows various BESS sizes, though 100% BESS ownership is assumed again [23]. Fortenbacher [10], formulated a centralized optimal dispatch algorithm for voltage and ampacity violation management that utilizes generation forecasting to determine allowable SOC trajectories for BESS systems, and applied this to an 18 load test feeder with 100% PV penetration. Though network voltage is adequately controlled, as in [12], it is assumed that every PV array is coupled to a BESS system. Real world trials of similar schemes are in planning, with an installation of 40 BESSs on an LV network in Barnsley, UK under development; the trial aims to investigate how LV PV hosting capacity may be increased by mitigating reverse flow, ampacity, and voltage rise events with BESSs [24].

Cost optimal BESS placement algorithms that utilize convex relaxation of the AC OPF problem [25], genetic algorithm and simulated annealing hybrids [9], and mixed integer linear programming [26], can be used to determine the theoretical lower bound for BESS placement and sizing. However, these algorithms have not been applied to the takeover of existing customer-owned BESSs, and so do not consider the likelihood that BESSs do not, or cannot, exist at every node on the simulated network.

Whilst all studies employed a valid test network for power flow simulations or BESS placement optimization, none considered how the feasibility of BESS control may change if their formulations were applied to networks characterised by high load count and load densities (with all except [12] studying feeder topologies with relatively low load counts by UK standards), and none considered how a change in the number of available BESSs may affect control feasibility. As a result we do not fully understand the extent to which customer owned BESSs may be used to mitigate LV network violations. Furthermore, whilst every study considered PV generation, we are not aware of any BESS dispatch studies that consider the effect of increased ASHP control on the feasibility of BESS based violation control. Though it is possible to solve utilization and voltage issues by fully or partially reconductoring an LV network [9], [26], only [9] compares this more conventional option to the BESS option, and this is limited to full network reconductoring.

In this study, we explore the feasibility of applying centralized and decentralized BESS dispatch algorithms for voltage and line capacity violation control on two urban LV feeders. We consider the situation in which the DNO may optimally select specific BESSs from a set of available customer owned BESSs, and determine how the size

of this set affects the likelihood of finding a feasible BESS solution at varying ASHP and PV ownership fractions. We also consider the likelihood of finding a reconductoring solution to violations, and where possible compare the cost of reconductoring to the cost of implementing a BESS dispatch scheme.

The primary objective of the study is to determine the extent to which BESS based control is feasible on UK LV networks, specifically where BESSs are static, customer owned systems, and are not necessarily present in the optimum quantity or locations. The secondary objective of the work is to gain a preliminary understanding of whether a customer BESS takeover scheme is likely to be able to compete economically with the reconductoring. The work contributes novel methodologies for the determination of optimal BESS takeover patterns (and for the determination of BESS control feasibility) under varying PV, ASHP, and BESS penetrations, and for the determination of optimal reconductoring patterns under coinciding high PV and ASHP penetrations.

Nomenclature

$\oslash$	Elementwise (Hadamard) division
$\boldsymbol{J}_{i,k}$	$i \times k$ vector of 1s
$\circ$	Elementwise (Hadamard) multiplication
$\mathbf{0}_{i,k}$	$i \times k$ vector of 0s
$\boldsymbol{c_{Com}}$	Compensation paid to customers for additional degradation associated with BESS takeover for ASHP demand limiting (£/BESS)
c_{Inc}	Incentive paid to customers for BESS takeover (£/BESS)
c_{DEG}	Cost per kWh of BESS degradation (£/kWh)
c_{kWh}	Per kWh cost of energy import for customers on standard tariffs (£/kWh)
c_{sys}	Cost of a BESS system (£)
$\boldsymbol{c}_{X^{Recon}}$	$n_c \times 1$ vector of conductor segment reinforcement costs
$c_{X_{Head}^{Recon,P}}$	Cost of reconductoring the feeder head line segment in parallel (£)
ΔC_{SC}	Cost of self-consumption reduction if changing from the SC algorithm to the FIL algorithm (£)
ΔC_{DEG}	Cost of degradation increase if changing from the SC algorithm to the FIL algorithm (£)
D_{FIL}	BESS degradation associated with operating in the FIL or ASHP demand limiting mode for the duration of either period (kWh)
D_{SC}	BESS degradation associated with operating in the self-consumption

	mode for the duration of either period (kWh)
$E_{i,t}^{Remain}$	Amount of energy remaining above the FIL for PV array i at time t for any given day. Remaining energy is predicted conservatively, and based on the 99th percentile for the given month (kWh)
EOL	Remaining fraction of initial BESS capacity at which BESS is considered to be at the end of its life (0 to 1).
$\boldsymbol{I}_{max}$	$n_\emptyset n_c \times 1$ per phase line segment ampacity limits (A)
$\Delta \boldsymbol{I}^{Recon}$	$n_l n_\emptyset \times 1$ vector of changes in line ampacity with existence of conductor replacement (A)
$\Delta \boldsymbol{I}_{Head}^{Recon,P}$	$n_l n_\emptyset \times 1$ sparse vector of changes in line ampacity with existence of feeder head line segment reconductoring (A)
L^C	Conductor Lifetime (years)
n_a	Number of ampacity monitor points
n_c	Total number of major line segments
n_l	Total number of residences
n_t	Number of time points in time series analysis
$n_{S,ASHP}$	Number of BESS takeovers required to solve a particular ASHP configuration
$n_{S,PV}$	Number of BESS takeovers required to solve a particular PV configuration
$\boldsymbol{P}_t^{Line}$	$n_\emptyset n_c \times 1$ vector of real power transfers across each phase of each ampacity monitor (centralized algorithm) or major line segment (all other uses) at time t (kW)
$P_{i,t}^d$	Real power demand on network by load i at time t (kW)
$P_{i,t}^g$	Real power inject by generator i at time t (kW)
$P_{i,MAX}^g$	The power rating of array i (kW)
$\boldsymbol{P}_{MAX}^g$	$n_l \times 1$ vector of $P_{i,MAX}^g$ values (kW)
$\boldsymbol{P}^{PV}$	$n_\emptyset n_c \times 1$ vector of real power on each phase across each major line segment, specifically in the PV simulation case (kW)
$\boldsymbol{P}^{HP}$	$n_\emptyset n_c \times 1$ vector of real power on each phase across each major line

	segment, specifically in the ASHP simulation case (kW)
$P_{i,t}^{s,FIL}$	Real power discharged by BESS i at time t (negative denotes charging), specifically in the FIL operation mode (kW)
$P_{i,t}^{s,SC}$	Real power discharged by BESS i at time t (negative denotes charging), specifically in the self-consumption operation mode (kW)
$P_{i,t}^{s}$	Real power discharged by BESS i at time t (negative denotes charging) (kW)
$\boldsymbol{P}_{t}^{s}$	$n_l \times 1$ vector of $P_{i,t}^{s}$ values at time t (kW)
$P_{i,t}^{s,Ch}$	Charging rate of BESS i at time t (kW)
$P_{i,t}^{s,Disch}$	Discharging rate of BESS i at time t (kW)
$\boldsymbol{P}_{lim}^{s}$	Maximum allowed BESS real discharge power (ASHP demand limiting operational mode only) (kW)
$Q_{i,t}^{s}$	Leading reactive power injected onto network by BESS i at time t (negative lagging) (kvar)
$\boldsymbol{Q}_{t}^{s}$	$n_l \times 1$ vector of $Q_{i,t}^{s}$ values at time t (kvar)
$\boldsymbol{Q}_{t}^{Line}$	$n_{\emptyset} n_c \times 1$ vector of reactive power transfers across each phase of each ampacity monitor (centralized algorithm) or line segment (all other uses) at time t (kvar)
$\boldsymbol{Q}^{PV}$	$n_{\emptyset} n_c \times 1$ vector of reactive power transfers across each phase of each major line segment, specifically in the PV simulation case (kvar)
$\boldsymbol{Q}^{HP}$	$n_{\emptyset} n_c \times 1$ vector of reactive power transfers across each phase of each major line segment, specifically in the ASHP simulation case (kvar)
S_i^{inv}	Total apparent power capacity of BESS inverter i (kVA)
$\boldsymbol{S}^{inv}$	$n_l \times 1$ vector of S_i^{inv} values (kVA)
$SOC_{i,t}$	State of charge of BESS i at time t (kWh)
SOC_{max}	Maximum allowed state of charge of a BESS (kWh)
t^{mag}	The magnitude of the timestep used in time series calculations (min)

$Traj_{i,t}^{max}$	Maximum trajectory; the maximum allowed SOC of BESS i at time t (kWh)
$\boldsymbol{V}^{PV}$	$n_{\emptyset}n_E \times 1$ vector of voltage magnitude values for each phase of each major line segment, specifically in the PV simulation (V)
$\boldsymbol{V}^{HP}$	$n_{\emptyset}n_E \times 1$ vector of voltage magnitude values for each phase of each major line segment, specifically in the ASHP simulation (V)
$\boldsymbol{V}_t^{Amp}$	$n_{\emptyset}n_a \times 1$ vector of voltages at each ampacity monitoring point at time t (V)
$\boldsymbol{V}_t^{End}$	$n_{\emptyset}n_e \times 1$ vector of voltages recorded on each phase of each endpoint monitor at time t (V)
$\boldsymbol{V}_{min}$	Vector of minimum allowable steady state voltage – 216.2 V ESQCR, with column length equal the number of monitoring points (V)
$\boldsymbol{V}_{max}$	$n_{\emptyset}n_c \times 1$ vector of maximum allowable steady state voltage – 253 V ESQCR, with column length equal the number of monitoring points (V)
$\boldsymbol{X}^{Recon}$	$n_c \times 1$ vector of binary variables representing the existence of reinforcement of major line segments
$\boldsymbol{X}^{S}$	$n_l \times 1$ vector of binary variables that denote the requirement for takeover of each BESS system
$X_{Head}^{Recon,P}$	Binary existence variable for parallel reconductoring along the feeder head line segment
$\boldsymbol{X}^{HP}$	$n_l \times 1$ vector of binary ASHP existence variables

2 Method

2.1 BESS control algorithms

The BESS placement formulations are developed in context with real time dispatch strategies, as the dispatch strategy significantly influences how BESSs must be placed and sized to ensure adequate control. Furthermore, the algorithms must be tested to determine how they alter self-consumption and BESS degradation, as a reduction in the former and increase in the latter may influence appropriate BESS takeover costs negatively (i.e. we may have to compensate customers for the negative effects the algorithms have on the operation and calendar life of their BESSs). The dispatch algorithms that the self-consumption, FIL, and centralized placement formulations are based on are described herein.

2.1.1 Self-consumption (SC)

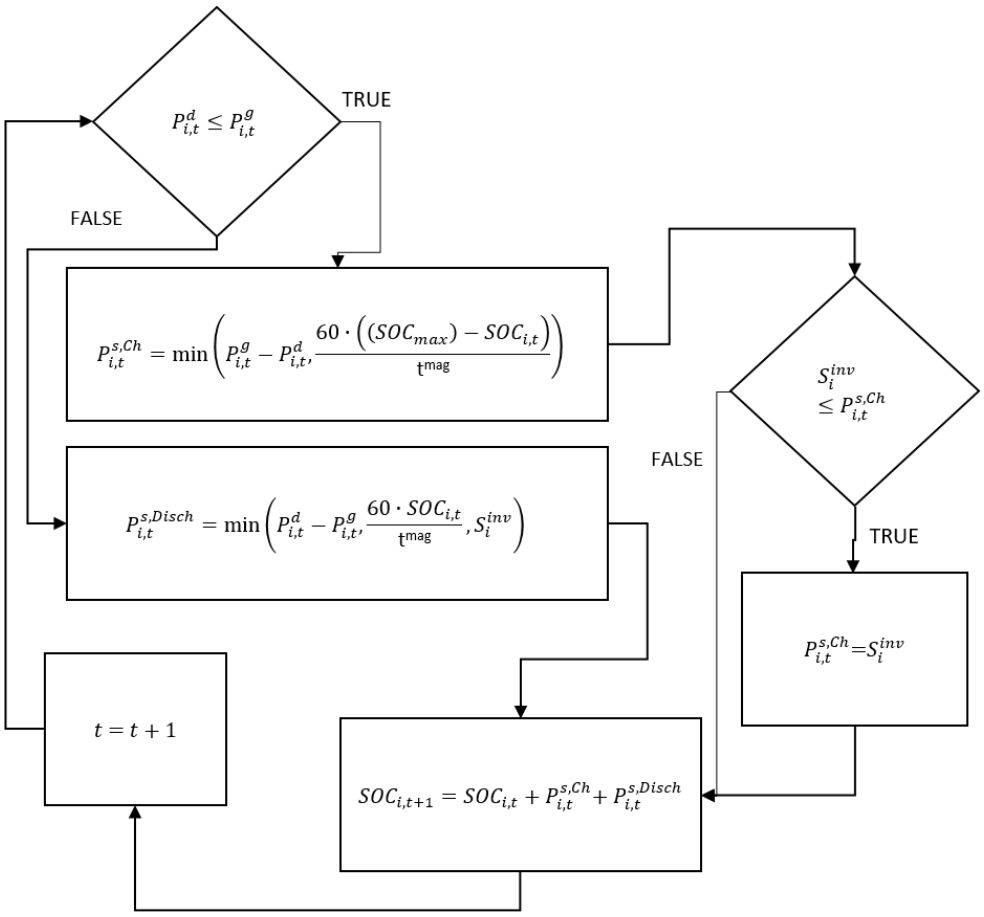

Fig. 1 – Flow chart mathematical representation of the SC algorithm.

The SC algorithm is used as a comparison to the proposed FIL algorithm, and represents typical residential PV-BESS system operation (fig. 1). When PV generation exceeds demand, the BESS charges at a rate equal to the excess generation, but is limited by the maximum inverter power and the remaining capacity of the BESS. When demand exceeds generation, the BESS discharges at a rate equal to the power demand, but is limited by the maximum inverter power and the quantity of energy remaining in the BESS.

2.1.2 FIL algorithm

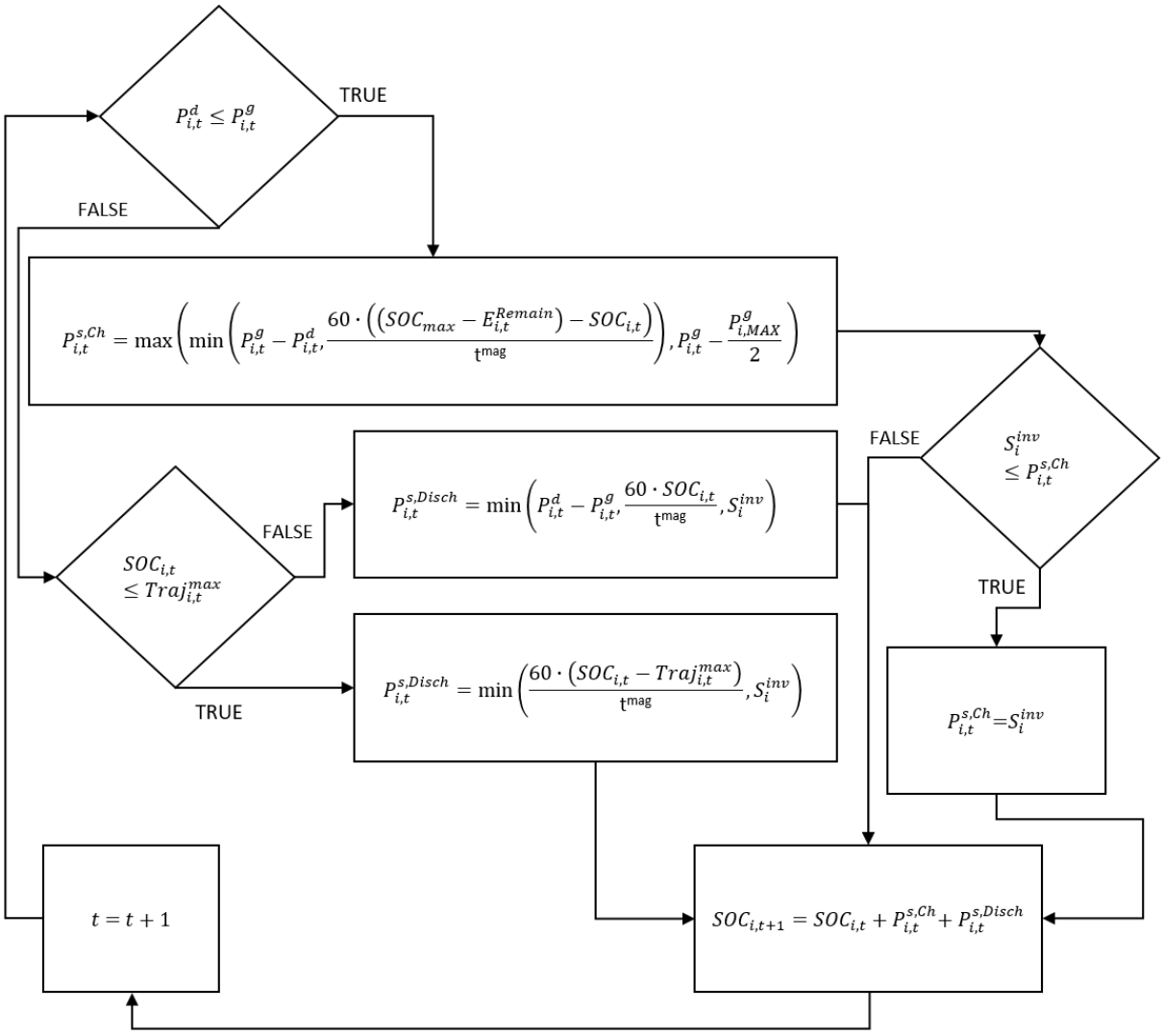

Fig. 2 – Flow chart mathematical representation of the FIL algorithm.

The FIL algorithm charges the BESS only when generation exceeds demand. Charging is first limited to the minimum of excess generation, or a charging rate that, if exceeded, risks the BESS reaching 100% SOC before the end of the daily generation period. Finally, charging is limited to maximum inverter power, S_i^{inv}.

When demand exceeds generation, the BESS discharges at the minimum of excess demand, maximum inverter power, or the discharge power that would cause the BESS to reach its minimum allowed SOC. If the BESS SOC exceeds the maximum allowed SOC trajectory at time period t, then it discharges at the rate required to bring

the SOC below this threshold. The maximum trajectory threshold ensures that BESSs have enough SOC headroom at the start of the next day to fulfil the export limiting duties that may be required. The control algorithm is shown in its mathematical form in fig. 2.

2.1.3 Centralized algorithm

The centralized algorithm controls BESSs as an ensemble using either a linear programming (LP) or quadratically constrained linear programming (QCLP) formulation (depending on how accurately line ampacity constraints need to be represented) that maximises overall self-consumption whilst preventing voltage and ampacity violations. The formulation that the centralized placement algorithm directly relates to is detailed in [26], though it could relate to any centralized dispatch algorithm that uses day ahead generation prediction to schedule violation mitigation dispatch strategy, for example [11].

2.2 Determination of customer incentive and penalty payments

In order to determine whether a change from the SC to the proposed FIL algorithm could be an economically viable option, we must consider whether the FIL algorithm significantly reduces customer self-consumption, or significantly increases BESS degradation. We determined the cost of self-consumption decrease by applying each of the SC and FIL algorithms to a series of 180 day, 5 min resolution generation and demand time series, then calculated self-consumption for a BESS i cost difference as,

$$\Delta C_{SC} = -c_{kWh}\left[\sum_{t=1}^{n_t} max\left(min\left(P_{i,t}^{g} + P_{i,t}^{s,FIL}, P_{i,t}^{d}\right), 0\right) - \sum_{t=1}^{n_t} max\left(min\left(P_{i,t}^{g} + P_{i,t}^{s,SC}, P_{i,t}^{d}\right), 0\right)\right] \quad (1)$$

The BESS degradation associated with each algorithm was determined by applying the SOC series generated during the previous step to the degradation estimation model presented by Xu [27], with rainflow-counting tasks performed using [28]. The cost to the customer associated with change in generation was then calculated as,

$$\Delta C_{DEG} = -c_{DEG}(D_{FIL} - D_{SC}) \quad (2)$$

Where c_{DEG} is the cost of 1 kWh of degradation,

$$c_{DEG} = \frac{c_{sys}}{SOC_{max} \cdot (1 - EOL)} \quad (3)$$

The calculation was applied for PV array sizes between 1 kWp and 4 kWp. Results showed either a marginal increase or decrease in self-consumption (depending on array rating) (fig. 3), and a significant decrease in degradation in all cases, which can be attributed to the lower average SOC experienced by each BESS in the FIL case. For this reason we assume switching from SC to FIL over months of high generation has no negative economic implications for the customer, and so the cost of takeover is assumed to be £25 per half annum (which is competitive with the annual takeover payment currently offered by MOIXA [29]).

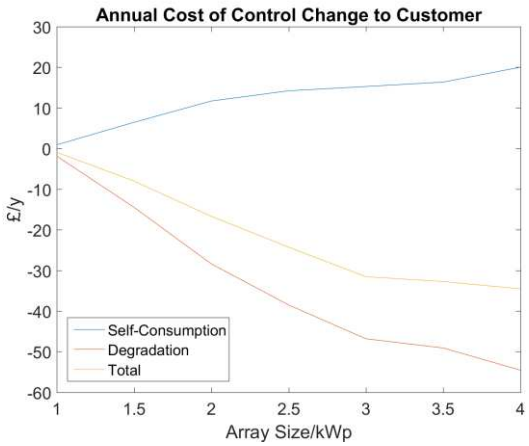

Fig. 3 – Shows the effective cost to the customer resulting from reduced self-consumption and increased cell degradation with a change from the SC to FIL algorithm. It can be seen that degradation decreases upon changing algorithm for all PV array sizes.

A comparison of the SC algorithm output to the data obtained from the centralized algorithm in our earlier work [26], showed that the centralized algorithm generally decreases self-consumption by £6 - 10 per annum, but also reduces degradation at a value of £30 - 50 per annum. This results from both the lower average SOC and the more conservative charging behaviour the algorithm tends to exhibit. We therefore assume a switch from the SC to centralized algorithm carries no negative financial implications to the customer.

We consider a payment of (£70 + £25) to any customer whom allows control takeover of their BESSs for ASHP demand limiting; this is equal to the additional degradation predicted for 3 months of cycling over the winter period (predicted using [27]), plus the half annum incentive.

Although the payments for takeover and the penalty payment for increased degradation in the ASHP case are reasoned, a lack of anecdotal real world data on the effectiveness of the cost incentive, and limited ASHP profile data means that both may vary from the chosen values, and so we consider how a higher than expected incentive payment and a lower than expected BESS degradation may affect the economics of a BESS based control system in section 4.

2.3 Placement formulations

The cost and technical feasibility of implementing BESS and reconductoring schemes is considered using 5 distinct optimization formulations:

- Centralized dispatch based BESS takeover
- FIL based BESS takeover
- ASHP demand limiting based BESS takeover
- Partial reconductoring
- Parallel partial reconductoring

Each formulation is explained herein.

2.3.1 Centralized dispatch based BESS takeover

BESSs are taken over under the assumption that feeder end voltages, line utilizations, and customer BESS operation can be remotely monitored by a central controller, and the optimum BESS setpoints for utilization and voltage control may then be calculated and communicated by the controller (using a control algorithm such as that presented in [10]). This has the advantage of providing a solution where decentralized control cannot, and generally requires a smaller BESS capacity, at the expense of monitoring and communication infrastructure that would not be required in a decentralized control scheme (e.g. FIL). Furthermore, the reliance on voltage as an input variable may affect the scalability of the scheme, as control of BESSs on different secondary substations (SSSs) may somewhat affect voltage conditions on the current network, resulting in oscillatory behaviour, and customer's BESSs do not necessarily experience the same operational pattern, resulting in variable self-consumption and BESS degradation.

Additional required monitoring costs are accounted for as in [26]. The algorithm is based on the placement and sizing heuristic developed in [26], and takes the form of a multiperiod mixed-integer quadratically constrained programming (MIQCP) problem with the objective of minimising the number of customer BESSs that the DNO/3rd party must take control of,

$$\min_{(\boldsymbol{X}^S)\in\mathbb{R}^{n_{l,1}}} \boldsymbol{J}_{n_{l,1}}^T \boldsymbol{X}^S \quad (4)$$

The minimisation is subject to numerous network and BESS constraints. Constraint (5) ensures voltage remains below the 253 V limit. The term $\boldsymbol{B}_{VP}\boldsymbol{P}_t^S + \boldsymbol{B}_{VQ}\boldsymbol{Q}_t^S$ calculates the change in voltage at each feeder end point with change in BESS real and reactive powers, and $\boldsymbol{V}_{max} - \boldsymbol{V}_t^{End}$ is voltage change required to bring the network voltage below the upper statutory limit. The linearized sensitivities of voltage magnitude to real and reactive power injects are used to predict end of line voltage changes with BESS operation, and are stored in the sensitivity matrices $\boldsymbol{B}_{VP}$ and $\boldsymbol{B}_{VQ}$. Their formulation and use is discussed in greater detail in [26].

$$\boldsymbol{B}_{VP}\boldsymbol{P}_t^S + \boldsymbol{B}_{VQ}\boldsymbol{Q}_t^S \leq \boldsymbol{V}_{max} - \boldsymbol{V}_t^{End} \quad (5)$$

Constraint (6) prevents line ampacity from exceeding the limit at monitored points, which are chosen based on potential for congestion. The term $\boldsymbol{P}_t^{Line} \oslash \boldsymbol{V}_t^{Amp} + (\boldsymbol{B}_{LP}\boldsymbol{P}_t^S) \oslash \boldsymbol{V}_t^{Amp}$ sums the contribution of generation,

demand and BESS systems to the current at each monitoring point, where the matrix $\boldsymbol{B}_{LP}$ maps BESSs to upstream monitoring points.

$$\sqrt{\left(\boldsymbol{P}_t^{Line} \oslash \boldsymbol{V}_t^{Amp} + (\boldsymbol{B}_{LP}\boldsymbol{P}_t^{S}) \oslash \boldsymbol{V}_t^{Amp}\right)^2 + \left(\boldsymbol{Q}_t^{Line} \oslash \boldsymbol{V}_t^{Amp} + (\boldsymbol{B}_{LQ}\boldsymbol{Q}_t^{S}) \oslash \boldsymbol{V}_t^{Amp}\right)^2} \leq \boldsymbol{I}_{max} \quad (6)$$

$$where,$$

$$\boldsymbol{B}_{LP} = \begin{bmatrix} \frac{\partial P_{1,1}}{\partial P_1^S} & \cdots & \frac{\partial P_{1,1}}{\partial P_i^S} & \cdots & \frac{\partial P_{1,1}}{\partial P_{n_l}^S} \\ \vdots & \ddots & \vdots & & \vdots \\ \frac{\partial P_{L,\emptyset}}{\partial P_1^S} & & \frac{\partial P_{L,\emptyset}}{\partial P_i^S} & & \frac{\partial P_{L,\emptyset}}{\partial P_{n_l}^S} \\ \vdots & & \vdots & \ddots & \vdots \\ \frac{\partial P_{n_a,n_\emptyset}}{\partial P_1^S} & \cdots & \frac{\partial P_{n_a,n_\emptyset}}{\partial P_i^S} & \cdots & \frac{\partial P_{n_a,n_\emptyset}}{\partial P_{n_l}^S} \end{bmatrix} \boldsymbol{B}_{LQ} = \begin{bmatrix} \frac{\partial Q_{1,1}}{\partial Q_1^S} & \cdots & \frac{\partial Q_{1,1}}{\partial Q_i^S} & \cdots & \frac{\partial Q_{1,1}}{\partial Q_{n_l}^S} \\ \vdots & \ddots & \vdots & & \vdots \\ \frac{\partial Q_{L,\emptyset}}{\partial Q_1^S} & & \frac{\partial Q_{L,\emptyset}}{\partial Q_i^S} & & \frac{\partial Q_{L,\emptyset}}{\partial Q_{n_l}^S} \\ \vdots & & \vdots & \ddots & \vdots \\ \frac{\partial Q_{n_a,n_\emptyset}}{\partial Q_1^S} & \cdots & \frac{\partial Q_{n_a,n_\emptyset}}{\partial Q_i^S} & \cdots & \frac{\partial Q_{n_a,n_\emptyset}}{\partial Q_{n_l}^S} \end{bmatrix}$$

It should be noted that this formulation uses voltages and ampacity recorded at monitor points, whereas all other formulations use values for every major line segment i.e. a greater number of points. This is because the centralized control algorithm relies on remote measurements during operation, whereas for all others we need simply to ensure that voltages can be held within limits during the placement stage, and we can therefore use as many monitoring points as desired with no concern as to whether these monitors would actually need to exist.

Each BESS inverter is constrained to a maximum total apparent power, and a minimum power factor. The formulation of these constraints can be found in [26]. BESS takeover variables are declared as binary, and are stored in $\boldsymbol{X}^S$**;** If a BESS is required to provide any power capacity at any time, then the takeover requirement is registered in $\boldsymbol{X}^S$ by changing the appropriate element from 0 to 1. Furthermore, BESS takeover may only occur where a BESS is already owned by a customer, is in suitable working condition, and the customer agrees to the takeover. In this study, this availability is predetermined randomly by forcing some elements of $\boldsymbol{X}^S$ to take the value 0, where the number of zero elements depends on the chosen BESS availability % for the given simulation (e.g. 25% of PV array owners will have zero BESS availability when BESS availability = 75%). We also include equality constraints to ensure that the SOC at each BESS at each time step is equal to the sum of charging events up to that point, and to prevent the SOC from falling below 0, or exceeding SOC_{max} during any time period.

2.3.2 FIL based BESS takeover

BESSs are placed under the assumption that there is no data communication between residences and centralized controllers, and BESSs primarily prevent the output of their associated PV array from exporting at more than half their rated power. This scheme has the advantages of avoiding communication and monitoring infrastructure costs, being independent of voltage i.e. stable to voltage changes on the wider grid, and treating customers BESSs consistently and proportionally to their PV array size.

$$\min_{(\boldsymbol{X}^S)\in\mathbb{R}^{n_{l,1}}} \boldsymbol{J}_{n_l,1}^T \boldsymbol{X}^S \quad (7)$$

The formulation is subject to the same voltage (5), ampacity (6), and control takeover constraints as the centralized scheme. However, BESS inverters do not provide reactive power, and charging is limited to inverter capacity (8), and to half of maximum PV generation (9). Furthermore, we do not consider energy constraints nor multiple time periods, as the assumed BESS has sufficient energy capacity to satisfy the FIL scheme on a clear sky summer day.

$$|\boldsymbol{P}_t^s| \leq \boldsymbol{S}^{inv} \quad (8)$$

$$-\frac{\mathbf{1}}{\mathbf{2}}\boldsymbol{P}_{\boldsymbol{max}}^{\boldsymbol{g}} \leq \boldsymbol{P}^{\boldsymbol{s}} \leq \mathbf{0}_{n_l,1} \quad (9)$$

As before, if any charging is requested of a BESS, the relevant element of the takeover requirement vector $\boldsymbol{X}^s$ is set to 1.

2.3.3 ASHP demand limiting BESS takeover

ASHP physical modelling data [30], developed using the methodology presented in [31], was made available by the University of Manchester's Electrical Energy and Power Systems group. The modelling assumes a cold, but not excessively cold UK winter day (min temp 0°C). From examination of this data it can be shown that, even for feeders with very high load counts (for which we would expect greater diversity), the ASHP load diversity factor approaches 1. Our takeover model therefore aims to procure enough BESSs to handle utilization or voltage violations during periods in which all ASHPs operate at nominal power.

The ASHP uses BESSs to limit the maximum demand of the pump under normal operation (i.e. without consideration of auxiliary heater operation), by discharging when the pump is operational. The formulation uses the objective function represented in equation (7). Constraint (10) ensures that a feasible solution has enough BESS capacity to ensure voltage can always be held above V_{min} (216.2 V), where $-(\boldsymbol{V}^{HP} - \boldsymbol{V}_{min})$ is the voltage

increase required to bring voltages at the end of each major line segment to within statutory limits, and $\boldsymbol{B}_{VP}\boldsymbol{P}^{S}$ represents the voltage change as a result of BESS operation

$$-(\boldsymbol{V}^{HP} - \boldsymbol{V}_{min}) \leq \boldsymbol{B}_{VP}\boldsymbol{P}^{S} \quad (10)$$

Constraint (11) limits BESSs to discharge at a rates no higher than those noted in $\boldsymbol{P}^{S}_{lim}$**;** this is equal to the bought capacity of the BESS in kWh (70% of total capacity in this study; chosen as compromise between energy capacity and degradation rate, which was seen to increase significantly when operating the BESS outside of this range) divided by the highest number of on hours observed from the provided dataset, which represents a typical cold UK day (12.5 hours for radiator based ASHP systems, and 13.5 hours for underfloor systems). This ensures all BESSs can operate for a full typical UK cold day without fully discharging, and takes a value of 0.69 kW for underfloor heating systems and 0.74 kW for radiator systems when we consider the 13.5 kWh BESS modelled in this study.

$$\boldsymbol{0}_{n_l,1} \leq \boldsymbol{P}^{S} \leq \boldsymbol{P}^{S}_{lim} \quad (11)$$

The formulation is also subject to constraints that ensure BESSs can only be taken over where BESSs exist (i.e. at selected residences that we have decided also own PV systems), and at residences where ASHP systems are installed. BESSs may not operate for reactive power control. If any discharging is requested of a BESS, the relevant element of the takeover requirement vector $\boldsymbol{X}^{S}$ is set to 1.

2.3.4 Partial reconductoring

Sections of the feeder main and lateral cables are replaced to bring feeder end voltages and line utilizations to within acceptable limits. The replacement cable properties are shown in table 1. The reconductoring model takes the form of a mixed integer linear programming (MILP) problem, with the objective of minimising the reconductoring cost. We simplify each feeder into a small set of cable segments - typically 3 - 5 for the main feeder path and 1 per branch, which we denote ‘major line segments’. This method is used because the computational burden of the MILP formulation is too high if we consider every meter of conductor; the number of simulations performed during this study is >10^6, and so problems must solve rapidly. Furthermore, it would be practically awkward to reconductor several very small sections of a feeder. The existence of reconductoring along each segment is stored in the vector of binary values, $\boldsymbol{X}^{Recon}$**.**

The objective function (12) minimises reconductoring cost by multiplying the binary value of the reconductoring variable for each segment by the cost of reconductoring that segment. The cost is a function of the segment length, and the number of service cables that branch from the segment.

$$\min_{(\boldsymbol{X}^{Recon} \in \mathbb{R}^{n_C \times 1})} \boldsymbol{c}_{X^{Recon}}{}^{T}\, \boldsymbol{X}^{Recon} \quad (12)$$

In this formulation, we consider both the violations that the networks PV arrays could cause during summer, and the violations that ASHPs could cause during winter simultaneously. This allows us to ensure that the chosen reconductoring pattern is sufficient to handle stresses caused by both technologies.

Constraint (13) ensures that line upgrades are sufficient to reduce peak voltages to 1.09 p.u. (250.7 V) at maximum PV generation, and constraint (14) ensures that line reinforcement is sufficient to ensure voltages do not fall below 0.94 p.u. (216.2 V) at maximum ASHP demand. The terms $\boldsymbol{B}_{Recon}^{PV}\boldsymbol{X}^{Recon}$ and $\boldsymbol{B}_{Recon}^{HP}\boldsymbol{X}^{Recon}$ represent the changes in voltage at the end of each major line segment (arising as a result of the chosen reconductoring pattern) at peak PV generation and ASHP demand respectively, and $\boldsymbol{V}_{max} - \boldsymbol{V}^{PV}$ and $-(\boldsymbol{V}^{HP} - \boldsymbol{V}_{min})$ denote the voltage changes required to bring the network within statutory limits in each instance. $\boldsymbol{B}_{Recon}^{PV}$ is a matrix that contains the expected voltage change at the end of each major line segment on each phase with respect to each reinforcement e.g. the (8,4)[th] element $\frac{\Delta V_{3,2}^{PV}}{\Delta X_4^{Recon}}$ denotes the expected voltage change at the end of major line segment 3 phase 2 when major line segment 4 is reconductored.

$$\boldsymbol{B}_{Recon}^{PV}\boldsymbol{X}^{Recon} \leq \boldsymbol{V}_{max} - \boldsymbol{V}^{PV} \quad (13)$$

$$-(\boldsymbol{V}^{HP} - \boldsymbol{V}_{min}) \leq \boldsymbol{B}_{Recon}^{HP}\boldsymbol{X}^{Recon} \quad (14)$$

$$where,$$

$$\boldsymbol{B}_{Recon}^{PV} = \begin{bmatrix} \frac{\Delta V_{1,1}^{PV}}{\Delta X_1^{Recon}} & \cdots & \frac{\Delta V_{1,1}^{PV}}{\Delta X_{n_C}^{Recon}} \\ \vdots & \ddots & \vdots \\ \frac{\Delta V_{n_E,n_\emptyset}^{PV}}{\Delta X_1^{Recon}} & \cdots & \frac{\Delta V_{n_E,n_\emptyset}^{PV}}{\Delta X_{n_C}^{c}} \end{bmatrix} \qquad \boldsymbol{B}_{Recon}^{HP} = \begin{bmatrix} \frac{\Delta V_{1,1}^{HP}}{\Delta X_1^{Recon}} & \cdots & \frac{\Delta V_{1,1}^{HP}}{\Delta X_{n_C}^{Recon}} \\ \vdots & \ddots & \vdots \\ \frac{\Delta V_{n_E,n_\emptyset}^{HP}}{\Delta X_1^{Recon}} & \cdots & \frac{\Delta V_{n_E,n_\emptyset}^{HP}}{\Delta X_{n_C}^{Recon}} \end{bmatrix}$$

Constraints (15) and (16) ensure that the current magnitude does not exceed the maximum cable ampacity rating, where $\sqrt{(\boldsymbol{P}^{PV} \oslash \boldsymbol{V}^{PV})^2 + (\boldsymbol{Q}^{PV} \oslash \boldsymbol{V}^{PV})^2}$ and $\sqrt{(\boldsymbol{P}^{HP} \oslash \boldsymbol{V}^{HP})^2 + (\boldsymbol{Q}^{HP} \oslash \boldsymbol{V}^{HP})^2}$ denote the current magnitude along each phase of each major line segment in the PV and ASHP cases respectively. $\boldsymbol{X}^{Recon} \circ \Delta\boldsymbol{I}^{Recon}$ is the increase in ampacity of each major line segment that results from the reconductoring pattern described by $\boldsymbol{X}^{Recon}$.

$$\sqrt{(\boldsymbol{P}^{PV} \oslash \boldsymbol{V}^{PV})^2 + (\boldsymbol{Q}^{PV} \oslash \boldsymbol{V}^{PV})^2} \leq \boldsymbol{I}_{max} + \boldsymbol{X}^{Recon} \circ \Delta\boldsymbol{I}^{Recon} \quad (15)$$

$$\sqrt{(\boldsymbol{P}^{HP} \oslash \boldsymbol{V}^{HP})^2 + (\boldsymbol{Q}^{HP} \oslash \boldsymbol{V}^{HP})^2} \leq \boldsymbol{I}_{max} + \boldsymbol{X}^{Recon} \circ \Delta\boldsymbol{I}^{Recon} \quad (16)$$

2.3.5 Parallel partial reconductoring

When the original reconductoring formulation fails to attain a feasible result, we consider allowing the head section of the feeder to be replaced with two parallel, equally sized conductors. The feeder head line segment

is defined as the length of feeder between the SSS and the first branch point. The cost of the addition of a parallel conductor is added to the objective function as $\boldsymbol{c}_{X_{Head}^{Recon,P}} X_{Head}^{Recon,P}$.

$$\min_{(\boldsymbol{X}^{Recon} \in \mathbb{R}^{n_C \times 1})} \boldsymbol{c}_{X^{Recon}}{}^{T} \boldsymbol{X}^{Recon} + c_{X_{Head}^{Recon,P}} X_{Head}^{Recon,P} \quad (17)$$

The voltage and ampacity constraints from section 2.3.4 are adjusted to allow for parallel reconductoring of the feeder head segment. $X_{Head}^{Recon,P} \boldsymbol{B}_{Recon,P}^{PV}$ is the voltage change at the end of each major line segment on each phase if parallel reconductoring on the feeder head segment exists, and zero otherwise. $X_{Head}^{Recon,P} \Delta \boldsymbol{I}_{Head}^{Recon,P}$ handles the change in ampacity of the feeder head segment if it is parallel reconductored, and has no effect otherwise.

$$\boldsymbol{B}_{Recon}^{PV} \boldsymbol{X}^{Recon} + X_{Head}^{Recon,P} \boldsymbol{B}_{Recon,P}^{PV} \leq \boldsymbol{V}_{max} - \boldsymbol{V}^{PV} \quad (18)$$

$$-(\boldsymbol{V}^{HP} - \boldsymbol{V}_{min}) \leq \boldsymbol{B}_{Recon}^{HP} \boldsymbol{X}^{Recon} + X_{Head}^{Recon,P} \boldsymbol{B}_{Recon,P}^{HP} \quad (19)$$

$$\sqrt{(\boldsymbol{P}^{PV} \oslash \boldsymbol{V}^{PV})^2 + (\boldsymbol{Q}^{PV} \oslash \boldsymbol{V}^{PV})^2} \leq \boldsymbol{I}_{max} + \boldsymbol{X}^{Recon} \circ \Delta \boldsymbol{I}^{Recon} + X_{Head}^{Recon,P} \Delta \boldsymbol{I}_{Head}^{Recon,P} \quad (20)$$

$$\sqrt{(\boldsymbol{P}^{HP} \oslash \boldsymbol{V}^{HP})^2 + (\boldsymbol{Q}^{HP} \oslash \boldsymbol{V}^{HP})^2} \leq \boldsymbol{I}_{max} + \boldsymbol{X}^{Recon} \circ \Delta \boldsymbol{I}^{Recon} + X_{Head}^{Recon,P} \Delta \boldsymbol{I}_{Head}^{Recon,P} \quad (21)$$

Where $\boldsymbol{B}_{Recon,P}^{PV}$ and $\boldsymbol{B}_{Recon,P}^{HP}$ are column vectors that contain the changes in voltage at the end of each major line segment when a parallel conductor is added to the head portion of the feeder.

Furthermore, parallel reconductoring may only occur if the original feeder head segment conductor has already been replaced, and both cables must have identical physical properties.

2.3.6 Iterative process

Because the above formulations involve linear approximations of non-linear sensitivities, there is usually some discrepancy between the model-predicted network state and that calculated using detailed AC power flow calculations, and this can result in a solution that falls slightly outside of the constraints. We therefore allow iteration until there is no change in the value of output variables, which in all cases explored in this work required 3 or fewer iterations.

2.4 Simulation scope

To understand the range of placement simulations performed, we must first define the nomenclature used to describe scenarios;

PV fraction - between 0 and 1, represents the fraction of residences with a PV array. The array ratings are assigned probabilistically based on UK installation size data, that suggests 1%, 8%, 13%, 15%, 14%, 12%, and 37% of systems are sized 1.0, 1.5, 2.0, 2.5, 3.0, 3.5 and 4.0 kWp respectively [32].

ASHP fraction - between 0 and 1, represents the fraction of residences with an ASHP system. ASHPs power ratings are based on physically modelled demand profiles developed in [31], where ASHPs serving radiator systems are rated at nominal 3 kW, and ASHPs serving underfloor heating systems (UHSs) are rated at nominal 2 kW.

BESS availability % - The percentage of PV owners that also own a BESS that is sufficiently sized and in good enough condition for the takeover scheme, and are willing to allow takeover of their BESS. We assume that PV array owners are the only residents who can own BESSs in this work, and that all available BESSs are sized at 13.2 kWh (matching the Tesla Powerwall 2 home BESS [13]), and the BESS is operated only in the SOC range 0 - 70%, in order to limit degradation.

PV/ASHP/BESS placement configuration – the specific location of each of the arrays/ASHPs/available BESSs e.g. at a PV fraction of 0.2 on a feeder with 75 residences, the entire set of PV placement configurations would represent every possible way to distribute 15 arrays between 75 residences.

We assess 50 different PV & ASHP placement configurations at each PV & ASHP fraction. Within each fraction, BESS availability at 25%, 50%, 75%, and 100% of PV sites is considered, and 30 different placement configurations of BESSs that are available for takeover are tested per PV & ASHP placement configuration – this is to account for the fact that in a customer owned BESS situation, the pattern of available BESSs may change over time for the following reasons;

- A residents BESS degrades to the point that it is of no use to the scheme, and it is not replaced.
- A resident who owns an operational BESS opts in/out of the scheme.
- A resident purchases a BESS and opts into the scheme.

These changes may affect the implementation costs and technical feasibility of a BESS solution.

The hierarchy of placement scenarios is show in fig. 4.

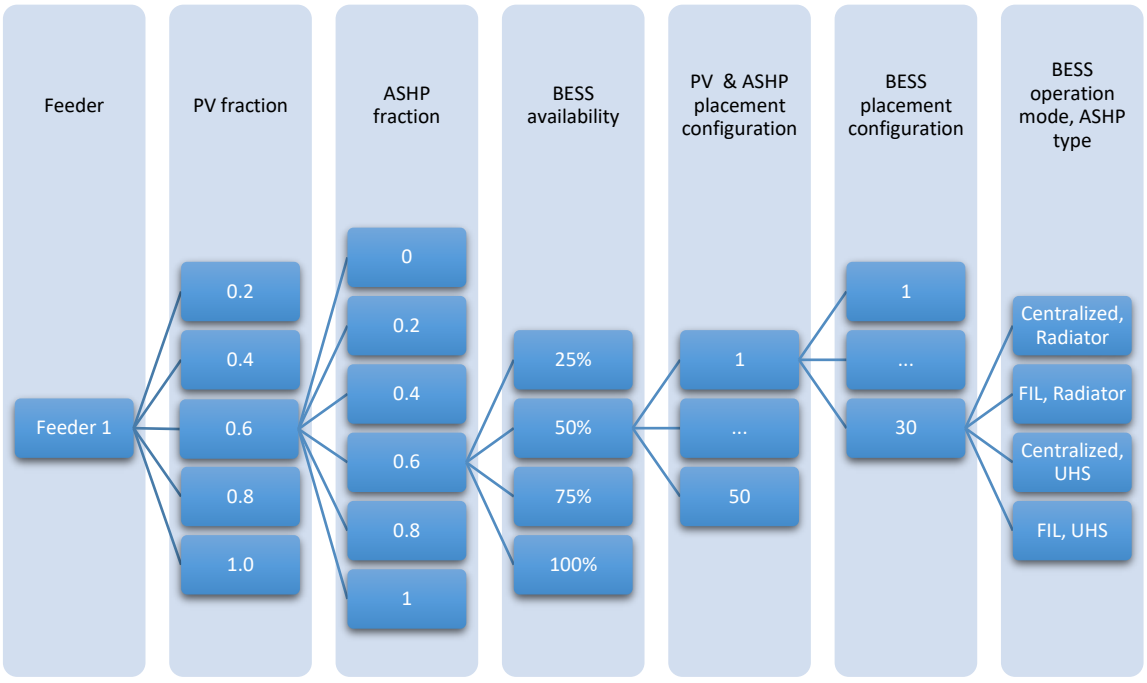

Fig. 4 – A hierarchal diagram of all simulation scenarios explored during this work.

The entire process is performed on models of two urban feeders (fig. 5). The feeder models were developed during the University of Manchester's low voltage networks solutions project, and represent real feeders located in the northwest of England. Feeder 1 serves 75 residences at a load density of 600 loads km^{-2}, whereas the much more heavily loaded feeder 2 serves 186 residences at a load density of 2100 loads km^{-2}. Both feeders experience voltage violations at renewables fractions <50%, but feeder 2 is much more vulnerable to thermal congestion than feeder 1. The feeder models are intended for use in 3Ø 4-wire unbalanced power flow simulations, and these are performed using openDSS. Voltages and ampacities calculated using openDSS can be fed into the optimization formulations developed in this study, allowing the iteration process (described in section 2.3.6) to proceed. All optimization problems are solved using IBM CPLEX.

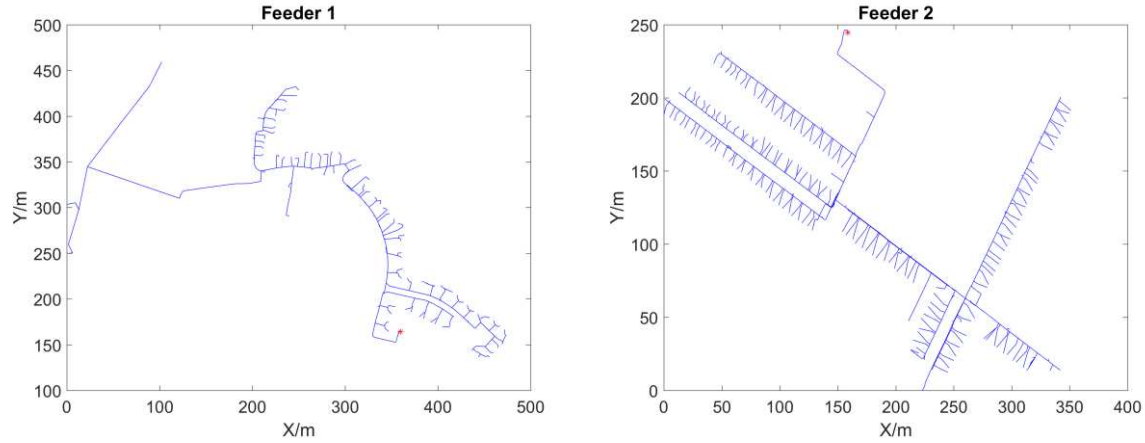

Fig. 5 – Topology of the 2 feeders examined in this study. The location of the SSS is, in each case, marked with an asterisk.

PARAMETER	VALUE	PARAMETER	VALUE
SOC_{max}	13.5 kWh (9.45 kWh used)	*Reconductoring cable cost*	£100 m^{-1} [33], [34]
S^{inv}	5 kVA [13]	*Service cable jointing charge*	£400 $Joint^{-1}$ [34]
c_{Com}	£70	*Reconductoring cable size*	300mm^2 [35]
BESS System CAPEX	£6500 [36]	*Reconductoring cable ampacity*	328 A (each Ø) [37]
c_{Inc}	£25	*Reconductoring cable* R_1	0.059 Ω m^{-1} [38]
Power factor	±0.85 [13]	*Reconductoring cable* X_1	0.067 Ω m^{-1} [38]
Conductor Lifetime	25 y [39]	*Reconductoring cable* R_0	0.215 Ω m^{-1} [38]
EOL	0.7 [13]	*Reconductoring cable* X_0	0.074 Ω m^{-1} [38]

Table 1 – Shows the input parameters for all simulations performed.

2.5 Analysis Methodology

We examine the solution to the reconductoring problem for every PV & ASHP placement configuration at every simulated renewables fraction level. If there is no solution for a given configuration, then we use the parallel reconductoring solution, along with its associated cost. In some situations, even parallel reconductoring cannot provide a solution, and this is discussed in section 3.2.

We then examine the BESS takeover problem for every BESS/PV/ASHP configuration. If there is no feasible solution to voltage and ampacity violations for a particular BESS configuration, then the PV & ASHP configuration that it is associated with is considered unsuitable for control with BESSs. A PV & ASHP placement is only considered suitable for BESS control when the voltage and ampacity violations it produces can be consistently removed by BESS control, regardless of the exact BESS configuration. It is important to understand that for any given model run, we solve for control under high PV penetration (using the models described in section 2.3.1 and section 2.3.2), then for control under high ASHP demand using the same set of available BESSs. This allows us to examine whether a network containing both PV arrays and ASHP simultaneously can cope with potential voltage and ampacity violations during both winter and summer months using a set pattern of BESS ownership.

Within each PV & ASHP fraction and BESS availability scenario, we count the number of PV & ASHP placements considered suitable for BESS control and report this figure as '% Success' for the given PV & ASHP fraction. For any PV & ASHP placement configurations suitable for BESS control that require >0 BESSs, we consider the cost to solve the same placement configuration with reconductoring, and determine the difference between costs as,

$$\Delta c = \frac{\boldsymbol{c}_{X^{Recon}}{}^{T}\boldsymbol{X}^{Recon}}{L^{C}} - c_{Inc}n_{S,PV} - (c_{Inc} + c_{Com})n_{S,ASHP} \quad (22)$$

Where we assume that L^C = 25 years. The resulting cost differentials are averaged and reported as 'Average annualized cost differential'. A value >0 suggests that takeover may be less expensive than reconductoring, whereas a value <0 suggests that reconductoring will likely be the cheaper option.

In the base case, we assume that the FIL based BESS algorithm is the dispatch algorithm, and that ASHPs sized at 3 kW serve a radiator system. We then examine the sensitivity of the effectiveness of BESS control to a change from the FIL algorithm to the centralized dispatch algorithm and a change from the 3 kW ASHPs serving radiators to 2 kW ASHPs serving underfloor heating systems. The sensitivity of economic feasibility to the changes in customer incentive, BESS system costs, degradation under the ASHP BESS control scheme, and conductor lifetime, are also considered.

3 Results

3.1 Feeder 1

The BESS takeover algorithm provided a possibility of solution to voltage and ampacity violations at up to 80% PV fraction and 40% ASHP, provided that every PV owner allows use of an adequate BESS. The maximum solvable PV fraction drops to 40% at 75% BESS availability (fig. 6). Below 50% BESS availability solutions only exist where the solution requires no BESSs, and therefore the BESS takeover method is useless unless the majority of PV system owners offer access to an adequate BESS.

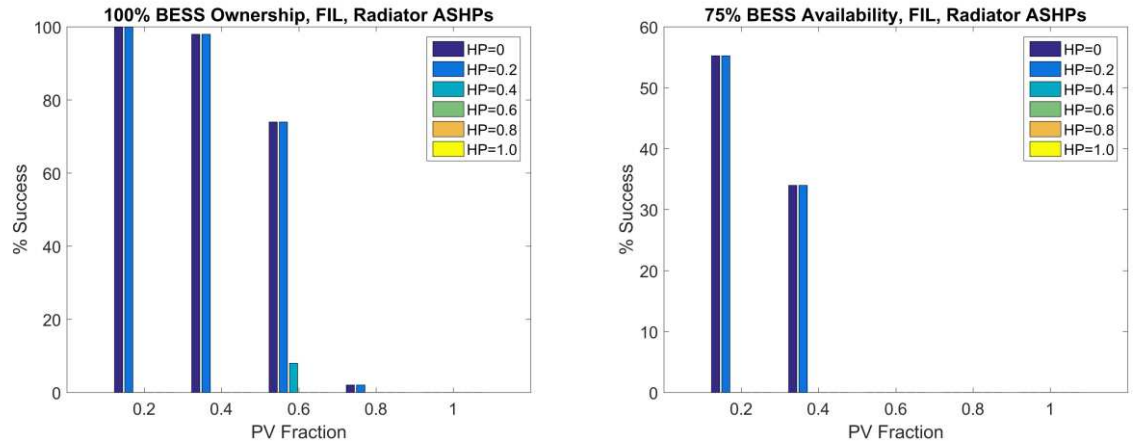

Fig. 6 - Average % success of the FIL BESS solution on feeder 1, where ASHPs are sized at 3 kW for radiator systems.

Considering the costs (table 1), we find that the takeover scheme is cheaper than the reconductoring alternative at low PV & ASHP penetrations (0 - 40%), suggesting that in a small set of circumstances the takeover scheme may provide an economically acceptable means to delay reconductoring (fig. 7). It should also be noted that BESS control appears cheaper in the 75% BESS availability case – this is because there are more solvable configurations in the 100% BESS availability case, and these additional configurations require a greater number of BESSs to solve, which increases the average solution cost.

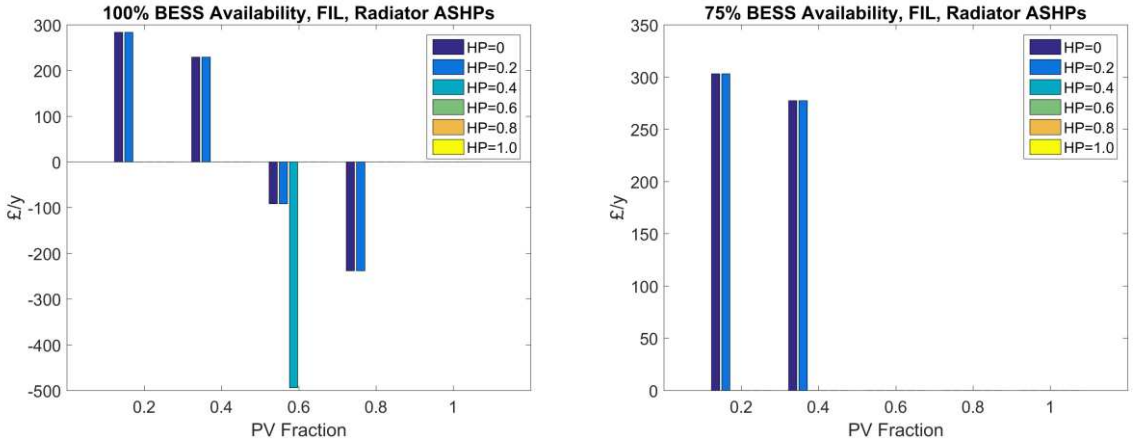

Fig. 7 - *Average annualized cost differential for feeder 1. If a BESS solution is technically infeasible for all of the placements tested within a given PV & ASHP penetration fraction, the bar representing this fraction is absent.*

Reconductoring adequately mitigates voltage and ampacity violations at all PV & ASHP fractions for 100% of simulations. Parallel reconductoring is never required.

3.2 Feeder 2

BESS FIL control was completely ineffective, with the probability of the existence of a successful BESS takeover pattern exceeding 0 on only 5 occasions (table 2), with control of ASHP violations failing above PV fraction = 0.2. In fact, a BESS takeover solution only exists in situations where the required BESS capacity equals zero, and fails wherever any violation is present.

		BESS ownership fraction			
PV ownership fraction		**0.25**	**0.5**	**0.75**	**1**
	0.2	100	100	100	100
	0.4	0	0	0	74

Table 2 - Shows % likelihood that a PV placement scenario can be solved with a given fraction of randomly located BESSs available for takeover. Table is equal for ASHP penetrations of 0 and 0.2, beyond which every element is equal to zero.

Reconductoring is always able to provide a solution to violations provided that the PV fraction is ≤ 0.8, and the ASHP fraction is ≤ 0.6, beyond this range reconductoring becomes less effective. This is entirely due to thermal congestion; even with parallel 300 mm^2 conductors, the maximum currents at PV fraction = 1 and ASHP fraction ≤ 0.8 can exceed the cable ratings (Table 3).

		ASHP ownership fraction					
PV ownership fraction		**0**	**0.2**	**0.4**	**0.6**	**0.8**	**1.0**
	0.2	100	100	100	100	32	0
	0.4	100	100	100	100	32	0
	0.6	100	100	100	100	32	0
	0.8	100	100	100	100	32	0
	1.0	36	36	36	36	12	0

Table 3 - Shows % success of reconductoring across all placement configurations at all tested PV & ASHP ownership fractions.

4 Sensitivity analysis

4.1 Change to centralized control

Adopting a centralized BESS control approach increases the likelihood of finding a feasible BESSs solution at all BESS availability fractions except 25% (fig. 8). BESS control cannot solve violation problems at high renewable fractions unless BESS availability exceeds 50%, suggesting that the BESS takeover method has limited scope with regards to this feeder. It should be noted that in the 100% availability case, and in various other scenarios

presented in this study, the % success for ASHPs increases with increasing PV penetration, which may appear counterintuitive. This is because the number of available BESSs increases with PV penetration in any given % availability scenario, so the likelihood of these BESSs being located at the same site as an ASHP does also. Consequently, ASHP hosting capacity increases.

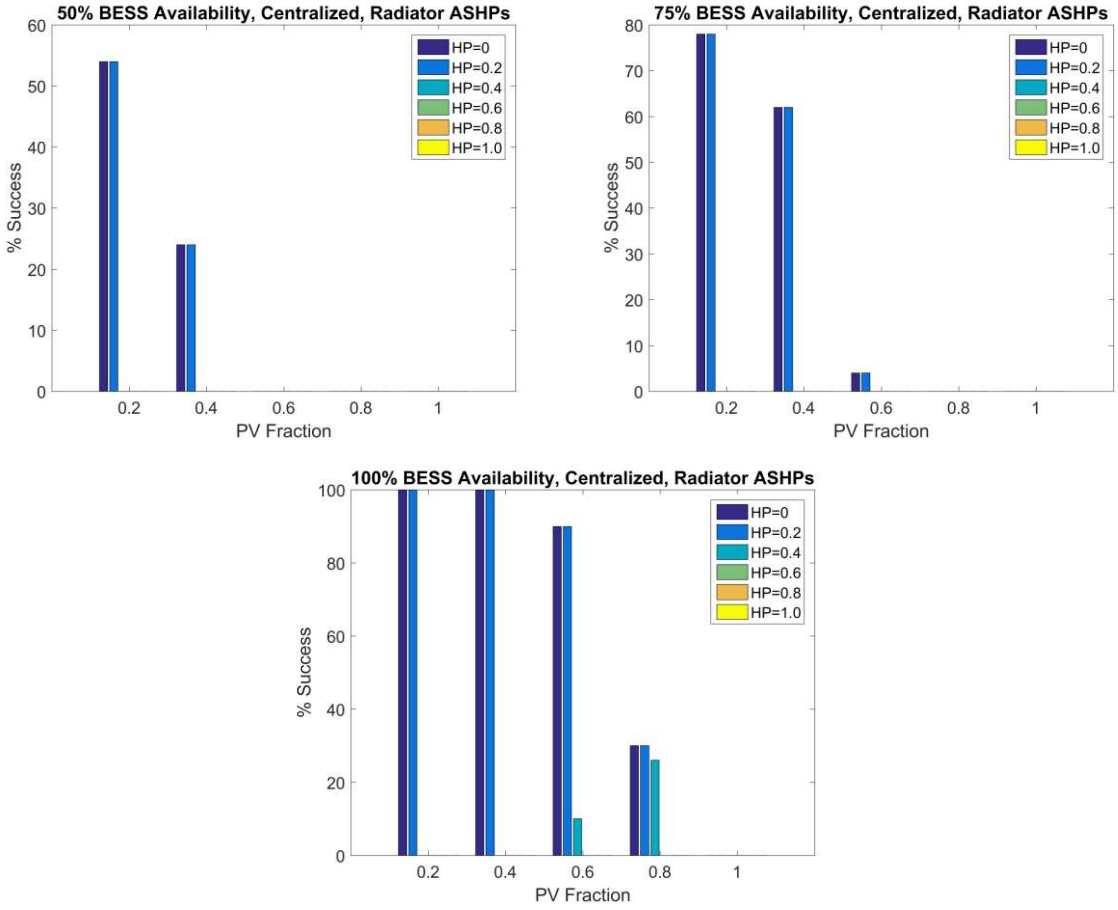

Fig. 8 - Average % success of the centralized BESS solution where ASHPs are sized at 3 kW for radiator systems on feeder 1

Furthermore, the additional cost of monitoring equipment results in average annualized costs that exceed those from the reconductoring and the FIL operation method (fig. 9). This is before the costs of data communication and processing are considered.

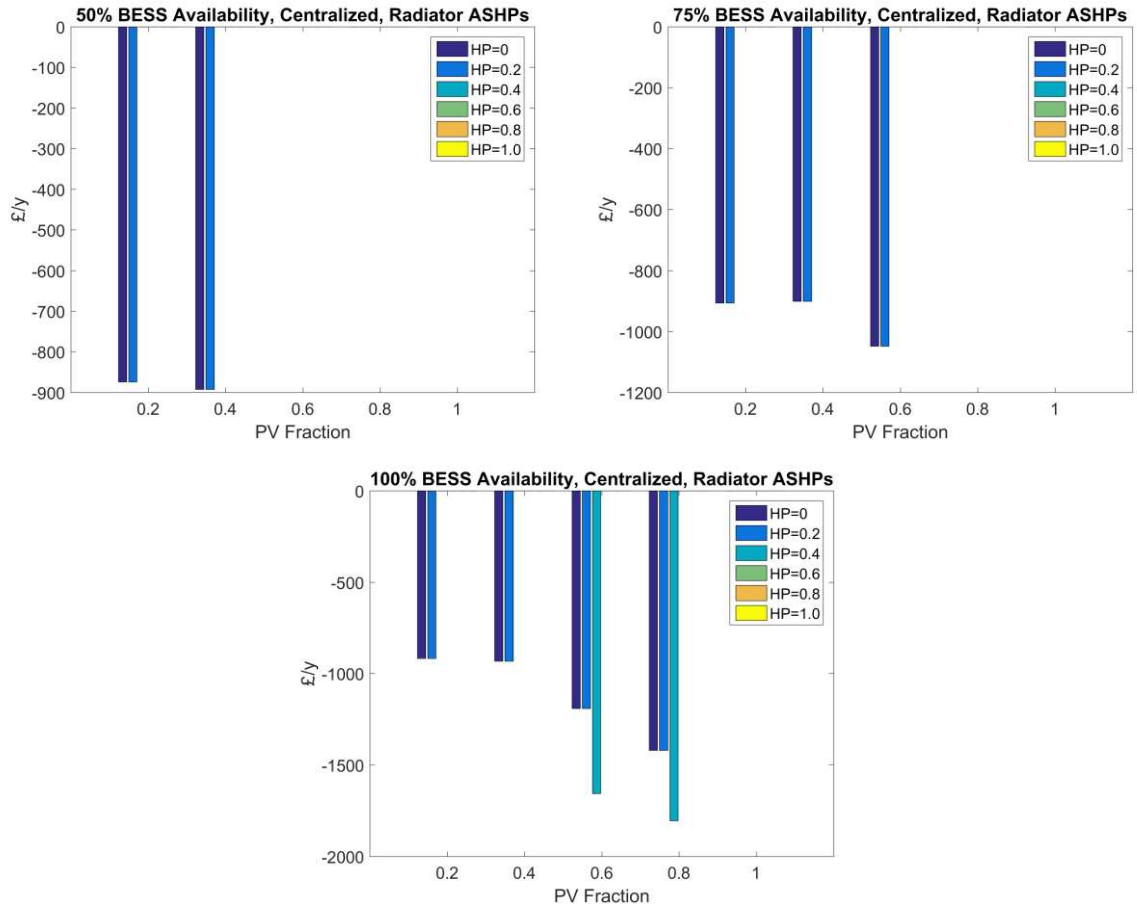

Fig. 9 - Average annualized cost differential for PV & ASHP configurations in which the centralized BESS and ASHP BESS models are able to provide a solution to violations on Feeder 1. ASHPs are sized at 3 kW for radiators.

4.2 Change to underfloor heating systems

The change to a lower power heating system allows an increase in maximum controllable ASHP fraction to 40% at 25% BESS availability, and 60% in some cases for higher BESS availabilities (fig. 10). In all cases of ASHP fraction ≤ 40%, the % success does not change between penetration levels, and this is because ASHP systems require no control at ownership fractions ≤40%, and require at least one BESSs for control at 60% ownership. There is never a feasible BESS control solution when ASHP ownership ≥ 80%. Where PV is no greater than 40%, BESSs takeover is typically cheaper than reconductoring where feasible (fig. 11), though a BESS solution is never guaranteed below 100% BESS availability.

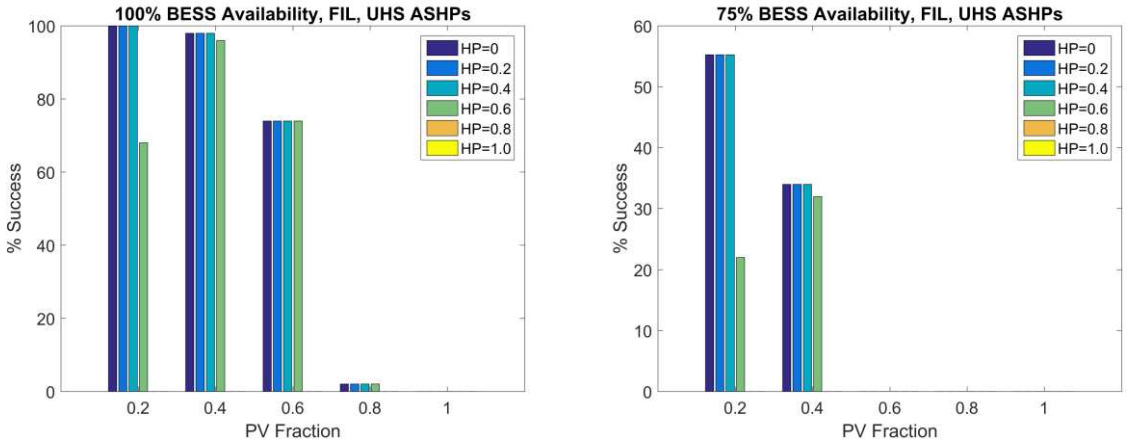

Fig. 10 - Average % success of the FIL BESS solution where ASHPs are sized at 2 kW for underfloor heating systems on feeder 1.

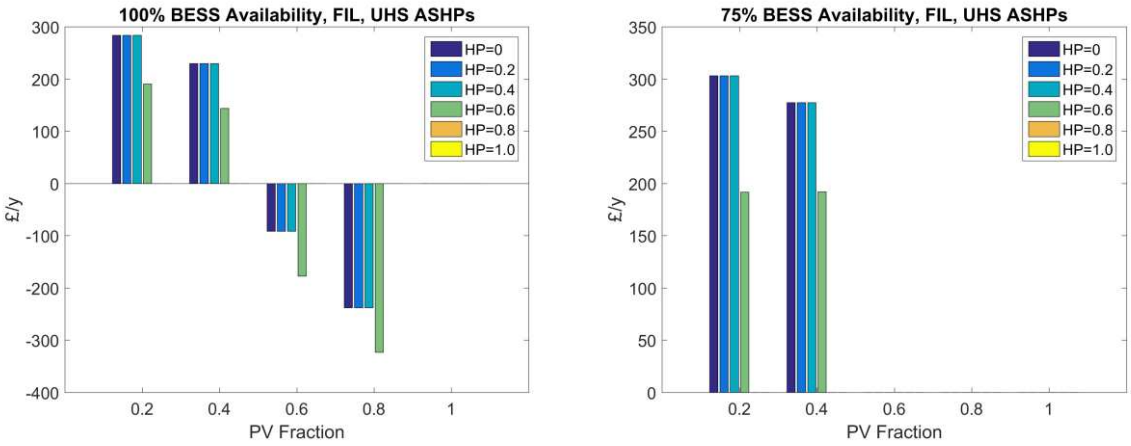

Fig. 11 - Average annualized cost differential for PV & ASHP configurations in which the FIL BESS and ASHP BESS models are able to provide a solution to violations on feeder 1, where the ASHPS are sized at 2 kW for radiators.

4.3 40 Year Reconductoring Lifetime

The 25 year conductor lifetime assumption is fairly conservative, and so we examine how average annualized cost differentials may change if we assume conductors have a 40 year lifetime. Whist the economic advantages of the BESS solution become more marginal, the BESS solution still proves cheaper than the reconductoring solution at PV & ASHP fractions ≤20%, provided that BESS availability % is very high (fig. 12).

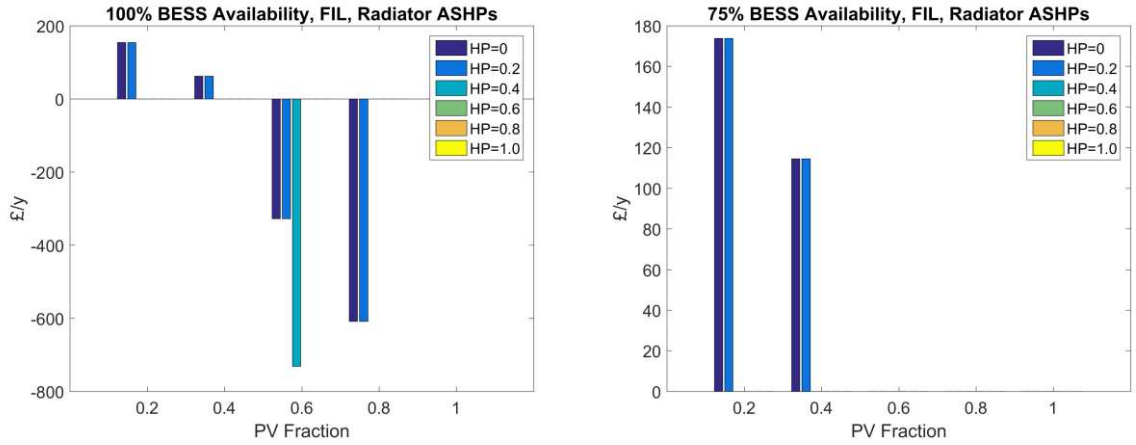

Fig. 12 - Average annualized cost differentials for feeder 1. A conductor lifetime of 40 years is assumed.

4.4 Half Expected BESS Degradation/Half BESS System Cost

A halved system cost or halved BESS degradation rate (and therefore halved penalty payment) has a small negative effect on differential costs at PV fraction = 0.6 and ASHP fraction = 0.2, with average cost reduction of £150 per annum. This small reduction results from a reduced compensation payment to an average of 4 customers. At any other PV fraction, ASHP fraction, or BESS availability below 100%, BESS control of ASHP-caused violations is either unrequired or impossible, so this change has no effect.

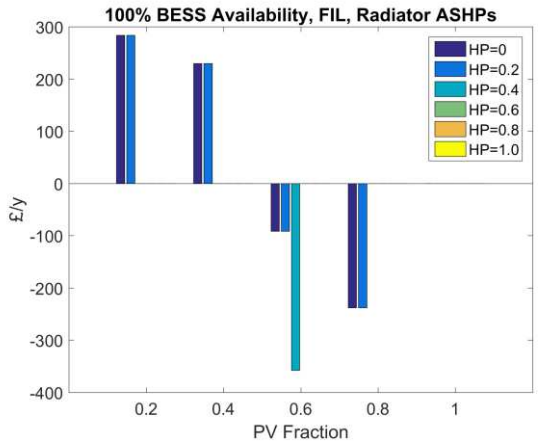

Fig. 13 - Average annualized cost differentials for PV & ASHP configurations in which the FIL BESS and ASHP BESS models are able to provide a solution to violations on network 1, and half the expected BESS degradation under ASHP demand limiting operation is assumed.

4.5 Increase in Customer Incentive Payment

If we assume a higher incentive of £40 (which reflects the higher end of Moixas proposed takeover incentive [29]), then BESSs takeover is only slightly more cost effective than reconductoring at PV fraction = 0.4. BESS takeover is still the most cost effective option at PV fraction = 0.2 (fig. 14), though violations only occurred in 4% of simulations at this penetration level.

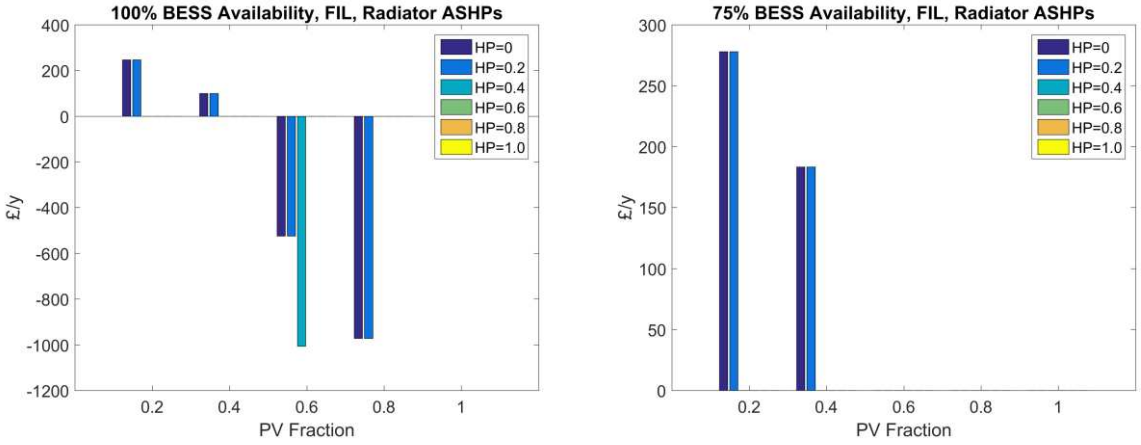

Fig. 14 - Average annualized cost differentials for PV & ASHP configurations in which the FIL BESS and ASHP BESS models are able to provide a solution to violations on Network 1, and an incentive cost increase from £25 - £40 is assumed.

4.6 Feeder 2 Sensitivity

If we takeover BESSs with the aim of controlling using the centralized dispatch algorithm, we observe exactly the same results as seen using the FIL algorithm, which further highlights the limited scope for the BESS takeover method.

If we assume all ASHPs are 2 kW and serve underfloor heating, results are unchanging from the base scenario. We cannot assess sensitivity of results to cost on this network, as no solutions to violations involve BESS control. In the reconductoring case, the reduced ASHP nominal power results in a $\frac{1}{3}$ ampacity reduction on the main portion of the feeder, meaning the congestion problem can now be solved at ASHP fraction = 1 (table 4).

		ASHP ownership fraction					
		0	**0.2**	**0.4**	**0.6**	**0.8**	**1.0**
PV ownership fraction	**0.2**	100	100	100	100	100	100
	0.4	100	100	100	100	100	100
	0.6	100	100	100	100	100	100
	0.8	100	100	100	100	100	100
	1.0	36	36	36	36	36	36

Table 4 - Shows % success of reconductoring across all placement configurations at all tested PV & ASHP ownership fractions in the case of underfloor, 2 kW ASHP systems.

5 Discussion

The relative ineffectiveness of BESS control in the ASHP case (when compared to PV generation case) can be rationalised by considering required operating times; BESSs may only need to operate for 2 hours to limit export during peak generation, whereas a cold day may require BESS operation for over 12 hours to limit ASHP demand. To ensure the BESS does not prematurely reach minimum SOC, it must discharge at a much lower power than it may charge in the PV case, thus limiting the efficacy of BESS control. Additionally, where BESS availability % < 100%, it is often seen that the existence of a BESS and ASHP at the same residence does not coincide, and therefore the demand of some ASHPs cannot be reduced.

Though the results suggest that long term violation management using customer owned BESSs is unlikely to be possible in BESS availability < 100% scenarios (and therefore we should not plan for this), if violations were seen to be occurring on an LV network, the DNO may be able to implement a BESS takeover scheme temporarily (provided that the configuration of PV, ASHPs, and available BESSs allows a BESS solution) to delay the need to reinforce – though this would require a very high incidence of available BESSs and a suitable network topology.

A change from the FIL to centralized algorithm increases the likelihood of a feasible solution at BESS availability %'s ≥ 50%, though no positive effect is observed at 25% availability. It is therefore clear that a high BESSs availability is required for any a benefit to emerge from an increase in algorithm complexity on feeder 1. On feeder 2, neither the FIL or centralized algorithms successfully increase the renewable hosting capacity of the network. This is a result of the low ampacity headroom at the feeder head in relation to the number of loads it serves; feeder 2 must serve 2.4 times the loads that feeder 1 must, with only 1.2 times the feeder head ampacity, and thus suffers thermal congestion issues at much lower renewables fractions.

The model described in this work determines the optimal reconductoring pattern for only one PV & ASHP configuration at a time i.e. we are solving the problem under the assumption that the placement already exists. Ideally, we would seek to expand this model to find an optimal reconductoring solution to multiple simultaneous PV & ASHP configurations, so that we could design reconductoring schemes that take uncertainty in future configurations into account. In reality, the takeover scheme is very unreliable at all BESS availabilities below

100%. Therefore within the scope of the current work there would be no real world benefit to the addition of predictive modelling, as reconductoring would always be chosen in practice over BESS control due to its much greater reliability.

The current work considers the mitigation of violations caused only by typical on-off cycle ASHP systems. However, there is a strong possibility that inverter driven variable capacity ASHPs will become the dominant technology in future. Because there is no available demand data for variable speed domestic ASHPs available, we consider the inclusion of such systems beyond the scope this study, with the aim to consider the technology when validated data becomes available. However, we do not believe that this is likely to change the outcome more than slightly, as variable ASHP systems still consume considerable power for the majority of heating periods during cold times (such systems are still only 10 - 15% more efficient than fixed speed systems during winter heating periods [40], [41]).

Whilst the work presented highlights the technical issues associated with implementing BESS based violation solutions on LV feeders, it does not quantitatively determine the correlation between feeder topology metrics and the viability of BESS based violation control, and so we aim to explore such correlations in future work.

6 Conclusion

This study has explored the feasibility of optimal customer owned BESS takeover for the prevention of voltage and line ampacity violations, and has introduced a set of MIQCP formulations to solving this problem. The formulations expand on previous work in the field by allowing low BESS uptake and non-ideal location of technologies i.e. our approach better approximates the non-optimal ownership conditions that may occur on future LV networks. The formulations should therefore be of greater practical use in network planning applications than those presented in previous works.

We have shown that, assuming a competitive customer incentive payment, the BESS solution could be less expensive than the reconductoring alternative in some low PV & ASHP penetration situations. However, violations could never be prevented on the 186 load network using BESSs, a BESS solution could not be guaranteed at any particular renewable penetration level on the 75 load network, and the reliability of BESS control fell substantially in all instances that BESS availability % fell below 100%. We therefore do not believe that behind-the-meter BESS control can be relied upon to delay reconductoring requirements in either the PV or ASHP case, though ongoing work will aim to quantify the correlation between network topology metrics and likelihood of BESS control viability.

Funding

This work was supported by the EPSRC [grant EP/L016818/1].

Acknowledgements

We would like to thank Dr Nicholas Good of the UoM Electrical Energy and Power Systems Group for providing the ASHP electrical demand profiles used in this study.

Conflicts of interest

None

7 References

[1] Dept. of BEIS, “Solar Photovoltaics Deployment in the UK December 2017.” Gov. UK, 2017.

[2] M. J. Hannon, “Raising the temperature of the UK heat pump market : Learning lessons from Finland,” *Energy Policy*, vol. 85, pp. 369–375, 2015.

[3] Ofgem, “Feed-In Tariff (FIT) rates,” 2017. [Online]. Available: https://www.ofgem.gov.uk/environmental-programmes/fit/fit-tariff-rates. [Accessed: 17-Jan-2018].

[4] Y. Xing *et al.*, “A review of concentrator silicon solar cells,” *Renew. Sustain. Energy Rev.*, vol. 51, pp. 1697–1708, 2015.

[5] S. Jana, U. Gangopadhyay, and S. Das, “State of the Art of Solar Photovoltaic Technology,” *J. Energy*, no. April, 2013.

[6] IRENA, “Renewable Power : Sharply Falling Generation Costs,” 2017.

[7] National Grid, “Future Energy Scenarios,” 2017.

[8] A. Navarro-Espinosa and L. F. Ochoa, “Probabilistic Impact Assessment of Low Carbon Technologies in LV Distribution Systems,” *IEEE Trans. Power Syst.*, vol. 31, no. 3, pp. 2192–2203, 2016.

[9] A. F. Crossland, “Application of stochastic and evolutionary methods to plan for the installation of energy storage in voltage constrained LV networks,” vol. 0, pp. 1–230, 2014.

[10] P. Fortenbacher, J. L. Mathieu, and G. Andersson, “Modeling and Optimal Operation of Distributed Battery Storage in Low Voltage Grids,” *IEEE Trans. Power Syst.*, 2017.

[11] P. Fortenbacher, G. Andersson, and J. L. Mathieu, “Optimal real-time control of multiple battery sets for power system applications,” *2015 IEEE Eindhoven PowerTech, PowerTech 2015*, 2015.

[12] A. T. Procopiou, “Active Management of PV-Rich Low Voltage Networks,” 2017.

[13] Tesla, “Powerwall 2 AC Specifications,” 2016.

[14] CCL, “Fronius Symo Hybrid 4kW Solar Inverter - Three Phase - 1 MPPT with Communication,” 2017. [Online]. Available: https://www.cclcomponents.com/fronius-symo-hybrid-4kw-solar-inverter-three-phase-1-mppt-with-communication?gclid=EAIaIQobChMIp9r-

8e_b1QIVATPTCh1yrQqxEAQYAiABEgJ0xfD_BwE. [Accessed: 18-Sep-2017].

[15] SMA, “Sunny Boy Storage 2.5.” .

[16] D. Rekioua and E. Matagne, *Optimization of Photovoltaic Power Systems - Modelization, Simulation and Control*, 1st ed. Springer, 2012.

[17] E. Isono, Y. Ebata, T. Isogai, and Hideki Hayashi, “Battery SCADA Demonstration System in YSCP,” in *22nd International Conference on Electricity Distribution*, 2013.

[18] M. G. Ippolito, E. Telaretti, G. Zizzo, and G. Graditi, “A New Device for the Control and the Connection to the Grid of Combined RES-based Generators and Electric Storage Systems,” in *4th International Conference on Clean Electrical Power: Renewable Energy Resources Impact*, 2013, pp. 262–267.

[19] R. Majumder, S. Chakrabarti, G. Ledwich, and A. Ghosh, “Advanced Battery Storage Control for an Autonomous Microgrid,” *Electr. Power Components Syst.*, vol. 41, no. 2, pp. 157–181, 2013.

[20] F. Marra, G. Yang, C. Træholt, J. Østergaard, and E. Larsen, “A decentralized storage strategy for residential feeders with photovoltaics,” *IEEE Trans. Smart Grid*, vol. 5, no. 2, pp. 974–981, 2014.

[21] Z. Wang, S. Member, H. Sun, and S. Member, “Distributed Storage Capacity Reservations for LV Network Operation,” pp. 1–5, 2015.

[22] I. Ranaweera and O. M. Midtgard, “Centralized control of energy storages for voltage support in low-voltage distribution grids,” *EEEIC 2016 - Int. Conf. Environ. Electr. Eng.*, 2016.

[23] F. Lamberti, V. Calderaro, V. Galdi, and G. Graditi, “Massive data analysis to assess PV / ESS integration in residential unbalanced LV networks to support voltage profiles,” *Electr. Power Syst. Res.*, vol. 143, pp. 206–214, 2017.

[24] Moixa, “Home battery trial aims to increase electricity network capacity to enable more solar homes and save £millions for customers,” 2017. [Online]. Available: http://www.moixa.com/press-release/home-battery-trial-aims-increase-electricity-network-capacity-enable-solar-homes-save-millions-customers/. [Accessed: 19-Dec-2017].

[25] A. Giannitrapani, S. Paoletti, A. Vicino, and D. Zarrilli, “Algorithms for placement and sizing of energy storage systems in low voltage networks,” *Proc. IEEE Conf. Decis. Control*, vol. 54rd IEEE, no. Cdc, pp. 3945–3950, 2015.

[26] R. C. Johnson, M. Mayfield, and S. B. M. Beck, “Optimal placement , sizing , and dispatch of multiple BES systems on UK low voltage residential networks,” *J. Energy Storage*, vol. 17, pp. 272–286, 2018.

[27] B. Xu, S. Member, A. Oudalov, and A. Ulbig, “Modeling of Lithium-Ion Battery Degradation for Cell Life Assessment,” vol. PP, no. 99, pp. 1949–3053, 2016.

[28] A. Nieslony, “Rainflow Counting Algorithm.” 2010.

[29] Moixa, “Moixa GridShare,” 2017. [Online]. Available: http://www.moixa.com/products/. [Accessed: 19-Dec-2017].

[30] N. Good, “Physically Modelled ASHP Data.” 2015.

[31] N. Good, L. Zhang, A. Navarro-Espinosa, and P. Mancarella, “Physical modeling of electro-thermal domestic heating systems with quantification of economic and environmental costs,” *IEEE EuroCon 2013*, no. July, pp. 1164–1171, 2013.

[32] A. Navarro-Espinosa and P. Mancarella, “Probabilistic modeling and assessment of the impact of electric heat pumps on low voltage distribution networks,” *Appl. Energy*, vol. 127, pp. 249–266, 2014.

[33] SSE, “Statement of methodology and charges for connection to southern electric power distribution plc.s electricity distribution system,” 2016.

[34] ENWL, “Stetement of methodology and charges for connection to electricicty noth west limited’s electricity distribution system,” 2016.

[35] ENWL, “Losses Strategy,” 2015.

[36] Solarguide, “Tesla Powerwall 2.0 Cost, Specs, and Reviews,” 2017. [Online]. Available: https://www.solarguide.co.uk/tesla-energy/powerwall-2. [Accessed: 19-Dec-2017].

[37] L. Protection and D. Systems, “Thermal Overload Protection of Cables,” pp. 1–6, 2005.

[38] A. Navarro-Espinosa and L. F. Ochoa, “Low Voltage Network Models.” 2015.

[39] Bahra Cables Company, “Low Voltage Power Cables,” 2011.

[40] R. S. Adhikari, N. Aste, M. Manfren, and D. Marini, “Energy Procedia Energy Savings through Variable Speed Compressor Heat Pump Systems,” vol. 14, pp. 1337–1342, 2012.

[41] F. J. Son, “Performance Testing of a Unitary Split-System Variable-Speed Heat Pump,” p. 5703, 2017.